

Materials Science

An Indian Journal

Full Paper

MSAIJ, 14(8), 2016 [307-315]

Roles of the matrix and of the primary carbides in the general high temperature oxidation behaviour of cobalt-based superalloys. part 3: the Co(10Ni,30Cr) matrix with tantalum carbides

Alexandre Navet¹, Albert Leroy¹, Thierry Schweitzer^{2,3}, Lionel Aranda^{2,3}, Patrice Berthod^{2,3*}, Elodie Conrath^{2,3}

¹Lycée Henri Loritz, 29 rue des Jardiniers, 54000 Nancy, (FRANCE)

²University of Lorraine, Faculty of Sciences and Technologies, (FRANCE)

³Institut Jean Lamour (UMR 7198), Team 206 "Surface and Interface, Chemical Reactivity of Materials"

B.P. 70239, 54506 Vandoeuvre-lès-Nancy, (FRANCE)

E-mail: patrice.berthod@univ-lorraine.fr

ABSTRACT

In this third and final part of this study dealing with the specific role of interdendritic carbides on the global high temperature oxidation behaviour of conventionally cast cobalt-based alloys, this was the one of a second type of carbides among the most commonly used for creep-resistance which was examined. Tantalum carbides present a better stability at high temperature than chromium carbides but their presence induces the one of a particularly oxidable element in high quantity and for some of them emerging from surface directly exposed to oxidation. The same tests of 46 hours at 1000, 1100 and 1200°C were applied to a Co-10Ni-30Cr-0.5C-7.5Ta alloy. They revealed that detectable oxidation during heating occurred sooner than for the two first studied alloys (Co-10Ni-30Cr and Co-10Ni-30Cr-0.5C). In addition, the isothermal mass gain – purely parabolic for this tantalum-containing alloy in contrast with the two others – was a little faster. And finally the scale spallation started at lower temperature than the ternary carbide-free alloy, as this was observed for the alloy containing chromium carbides.

© 2016 Trade Science Inc. - INDIA

KEYWORDS

Cobalt alloy;
Tantalum carbides;
High temperature oxidation;
Oxide spallation.

INTRODUCTION

To achieve very high mechanical properties including creep-resistance in equi-axed cast cobalt-based superalloys to make them usable at elevated temperature, besides solid solution strengthening and secondary carbides precipitated in the matrix as fine particles^[1-4], it may be compulsory to involve carbides

too. This maybe efficiently done by promoting the formation of script-like very stable carbides in the interdendritic spaces where there are closely mixed with the outer parts of the dendritic matrix. Among the most stable carbides possibly appearing with such morphology and such localization there are the tantalum carbides. They can be effectively obtained exclusively as script-like TaC forming an eutectic with matrix, in

Full Paper

cobalt-based^[5,6] alloys as well as in other systems as Fe-based alloys⁷, Fe-Ni-based alloy^[8]... but not in other ones such as Ni-based alloys^[9].

Even if Cr, another important carbide-former element is also present and this in much higher quantities than tantalum, the TaC phase forms preferentially to chromium carbides. Furthermore the TaC carbides keep their script-like shape on rather long times at not too high temperature, with as result a good sustainability of their strengthening effect. However it is true that with time spent at high temperature they tend to become more and more fragmented with consequently significant evolution of the properties of the alloys, in the mechanical^[10], thermomechanical^[11] and high temperature oxidation^[12] domains.

In some commercial equi-axed cast cobalt-based superalloys, such as Mar-M509, the tantalum carbides are present together with chromium carbides in the interdendritic spaces. This allows achieving significant strengthening of the alloys at high temperature without too high cost. However, to obtain a sufficiently developed interdendritic carbides network rather high quantities of tantalum must be added, which may lead to more than 5 wt.% Ta for more than 0.35-0.4 wt.% C. Such alloys maybe particularly creep-resistant at high temperature. But the presence of so high content in a so high reactive element as Ta, moreover concentrated in the emerging interdendritic spaces (eutectic TaC), may deeply influence the behaviour of the alloys at high temperature, not only in isothermal conditions, but also during the heating and the cooling.

In a previous study the behaviour in oxidation at high temperature of a ternary alloy Co-10Ni-30Cr, simulating the base of many cobalt-based superalloys, was entirely characterize during the whole thermal cycle of a thermogravimetric test: heating at constant rate, isothermal stage, cooling at constant rate¹³. In a first time these preliminary results acted as comparison base to try specifying the isolated role of chromium carbides on the high temperature oxidation of a quaternary alloy Co-10Ni-30Cr-0.5C containing such chromium carbides. Here the same results issued from the characterization of the oxidation of the ternary alloy will act as a comparison base for a TaC-reinforced cobalt-based superalloys containing the same quantities of nickel and of chromium as this ternary alloy. Since the

alloy which will be studied here is double-phased – a dendritic matrix and a carbide network made of TaC only – this comparison will show the specific role of these tantalum carbides, even if a little part of Ta is present in solid solution in its matrix.

The effect of the presence of TaC carbides will be thereafter compared to the one of chromium carbides. In addition, a comparison between the Co(Ni)-30Cr-0.5C alloy and two alloys of similar compositions in Cr (25wt.%) and C (0.5wt.%) and based on Co only or Ni only, will enrich this last part of the study.

EXPERIMENTAL

A Co-10Ni-30Cr-0.5C-7.5Ta (all contents being in wt.%) was previously used in two recent works^{14,15} to study the effect of water vapour on the high temperature oxidation of cobalt-based alloys in a furnace. This alloy was here considered again (microstructure reminded in Figure 0: dendritic matrix in grey and interdendritic tantalum carbides in white). The not used parts were machined, to obtain three parallelepipeds of about 3mm × 7 mm × 7 mm, which were ground with SiC papers of grade 1200. The edges and corners were smoothed. The oxidation tests were realized in dry synthetic air (80% N₂-20% O₂) using a SETARAM TGA92 92-16.18 thermobalance. The heating was realized at +20K min⁻¹, the isothermal stage at 1000, 1100 or 1200°C during 40 hours, and the cooling rate at -5K min⁻¹.

The mass variations were recorded every 12.2 (test

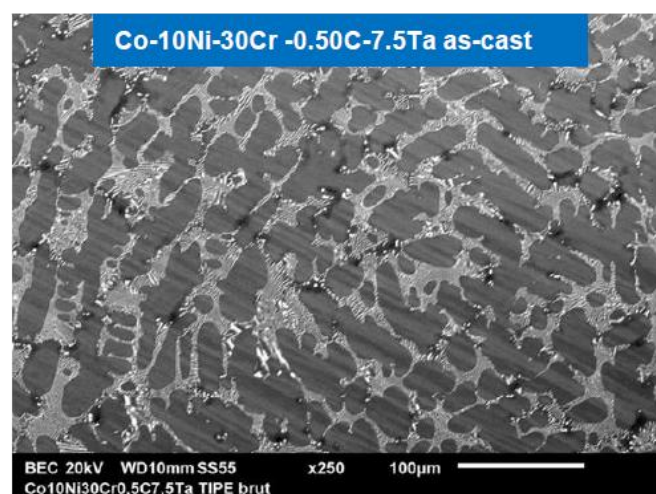


Figure 0 : SEM/BSE micrograph illustrating the as-cast microstructure of the studied alloy

at 1000°C), 12.3 (test at 1100°C) or 12.4 (test at 1200°C) seconds. The mass gain files were corrected from the air buoyancy variations and plotted as mass gain versus temperature and exploited to specify the following characteristics:

Heating

- temperature at which the mass gain is significant enough to be detected by the micro-balance
- eventual determination of the activation energy (if linear part in the curve describing the instantaneous linear mass gain rate variation with temperature, plotted according to the Arrhenius scheme)
- total mass gain achieved during the whole heating between the start of oxidation and the beginning of the isothermal stage)
- final linear mass gain rate when temperature reaches the isothermal stage one

Isothermal stage

- global shape of the mass gain curve when plotted versus time (parabolic or not, jumps or not)
- total mass gain exclusively achieved during the isothermal stage

Cooling

- Temperature at which the mass variation accelerates or becomes irregular (start of scale spallation)
- final mass variation

RESULTS AND DISCUSSION

Oxidation during heating

The heating parts of the mass gain curves plotted versus temperature are presented together in Figure 1. It appears first that the common parts of the 1000°C-curve and the 1100°C-curve are almost superposed. This is not clear for the 1200°C curve since an artefact is visible in the heating curve. These three curves show that the mass gain by oxidation during the heating has become high enough to be detected by the used thermo-balance at a temperature which presents a bad reproducibility since the three values are spread over 780 - 900°C (TABLE 1).

Over these temperatures of oxidation start the instantaneous linear kinetic constant increases more and more rapidly when temperature increases during the

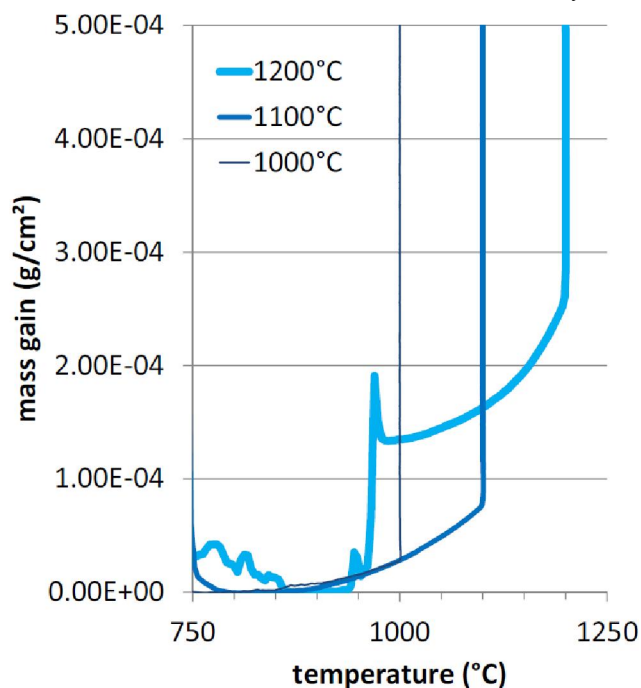


Figure 1 : Enlarged view of the mass gain curves recorded during heating until reaching 1000, 1100 or 1200°C

TABLE 1 : Values of the temperatures (in °C) at which the mass gain by oxidation during heating has become significantly high enough (*: probable problem during the mass gain recording)

1000°C- test	1100°C- test	1200°C- test	reproducibility
774.96	834.59	903.35*	bad

heating, this letting thinking to an exponential increase with temperature. The Arrhenius plot (Figure 2) confirms this over the whole heating from oxidation start or only on the high temperature part of the heating, since the points' clouds are globally elongated along a straight line. The slope of the regression straight line led to the values of activation energies listed in the first line of TABLE 2. These values are variable (between 60 and 200 kJ Mol⁻¹), maybe because different oxidation sequences occurring during the heating, at successive temperature levels, such as oxidation of cobalt, of tantalum or of chromium.

The second line of TABLE 2 presents the values of the final value of $d(\Delta m/S)/dt$ when temperature reaches the stage temperature. This final value of K_1 effectively increases with temperature, showing that oxidation is, at the beginning of the isothermal stage, logically faster when the stabilized temperature is higher. The values of the mass gains achieved during the whole heating are

Full Paper

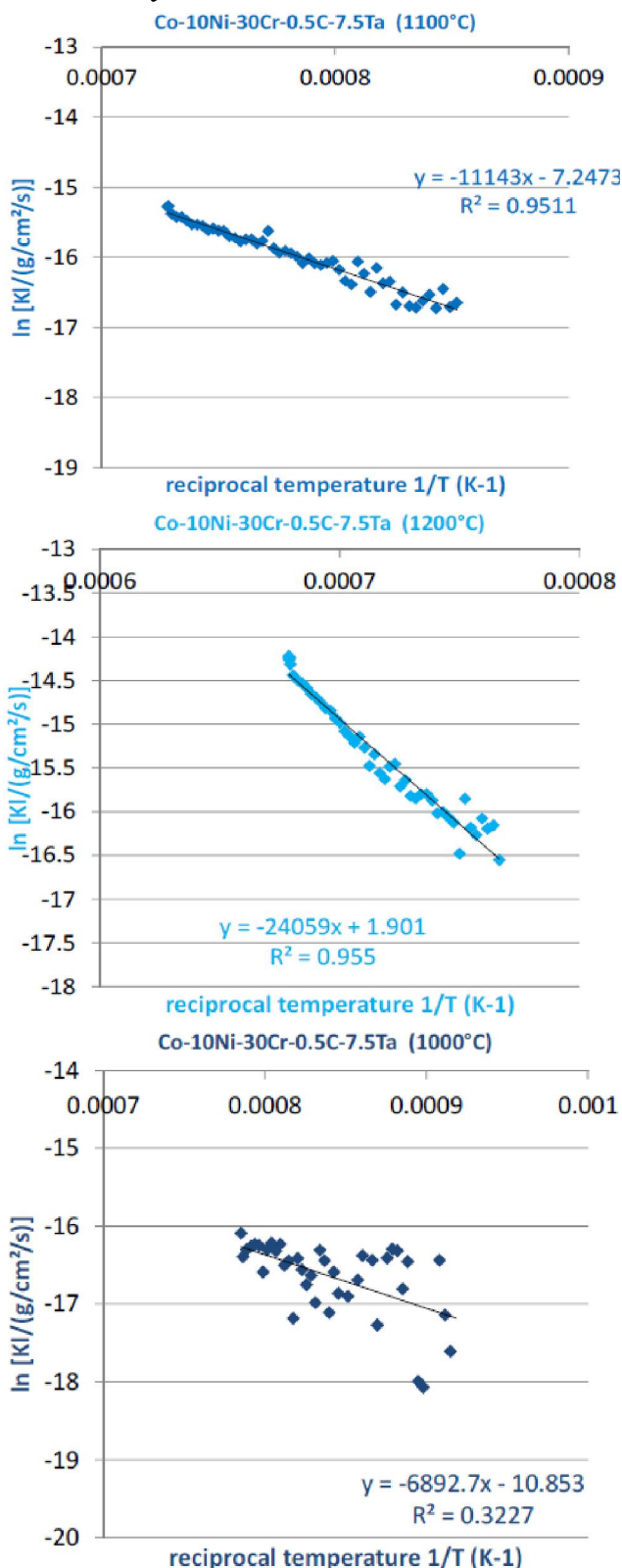


Figure 2 : Arrhenius plot of the instantaneous linear oxidation constant over the whole heating (or only a part if the point's cloud is not straight elongated); values of the slope of the regression straight line for deducing the values of activation energies (displayed in TABLE 2)

TABLE 2 : Values of the activation energies characterizing the dependence on temperature of the linear oxidation constant K_l issued from the successive values of K_l noted during the heating (over the linear part of the Arrhenius plot); value of the K_l value at the start of the isothermal stage

Q (J/Mol) issued from the $\ln((d\Delta m/S)/dt)$ plot versus $1/T$ (K) during heating	1000°C- test	1100°C- test	1200°C- test
	57306	92643	200027
Final value of K_l (end of cooling, beginning of the isothermal stage ($\times 10^{-8}$ g/cm ² /s))	11.04	21.70	69.55
Mass gain at the end of heating (mg/cm ²)	0.028	0.080	0.292

TABLE 3 : Values of the temperatures at which the mass gain by oxidation during heating has become significantly high enough to be detected by the thermobalance

Oxidation test	Mass gain at the end of heating (mg/cm ²); Proportion / heat.+isoth. (%)	Mass gain at the end of the isoth. Stage (mg/cm ²) (sum of ← and →)	Isothermal mass gain (mg/cm ²); Proportion / heat.+isoth. (%)
1200°C- test	0.292 (5.85%)	4.992	4.700 (94.15%)
1100°C- test	0.080 (2.66%)	3.004	2.924 (97.34%)
1000°C- test	0.028 (2.15%)	1.323	1.295 (97.85%)

displayed in the third line of TABLE 2. They are also logically higher for a higher temperature.

Isothermal oxidation

When plotted as mass gain versus time the three isothermal oxidation curves (stage temperatures 1000, 1100 and 1200°C) are completely parabolic, with no significant jumps. The mass gains achieved during the isothermal stage are given for the three temperatures in the last column of TABLE 3. Logically the higher the stage temperature the higher the isothermal mass gain and, after addition of the mass gain achieved during heating (values reminded in the first results column of TABLE 3 again), the higher the total mass gain realized before cooling started (middle column).

Phenomena at cooling

At the end of the isothermal stage the temperature

TABLE 4 : Values of the temperatures at which spallation started during the cooling and final mass variation after return at room temperature

Oxidation test	Temperature of start of the cooling induced scale spallation (°C)	Final mass variation at the end of the whole thermal cycle (mg/cm ²)
1200°C-test	883.53	-3.847
1100°C-test	806.03	-2.00
1000°C-test	550.92	+2.48

decreased with a slow linear rate. At a given temperature the decrease in mass gain started then accelerated, the curve becoming more or less irregular. The values of the temperatures at which the oxide scale spallation phenomenon started, red on the curves, are given in the first results column of TABLE 4.

The temperature at which the oxide spallation starts depends on the temperature of the isothermal stage. Indeed, during the cooling from 1200°C the scale spallation started at a temperature which is higher than for the cooling after the stage at 1100°C. The same order of scale spallation start temperature exists between the cooling from 1100°C and the one from 1000°C.

Graphical summary

The whole curves plotted as mass gain versus

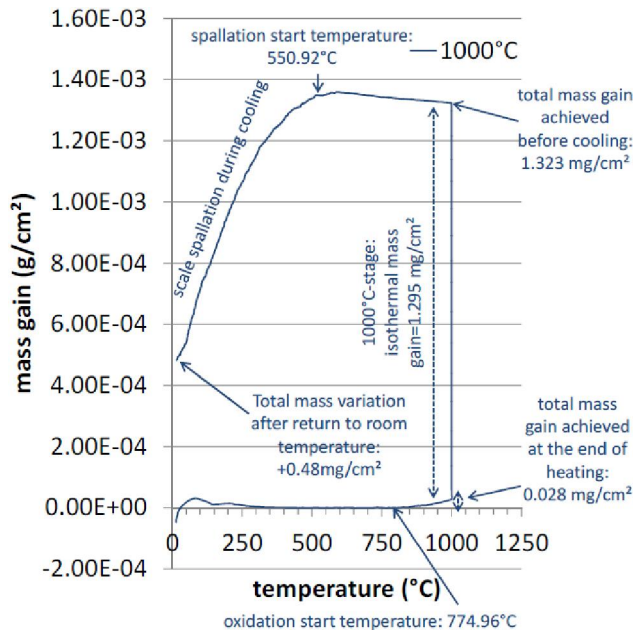


Figure 3 : The {mass gain versus temperature}-plot for the whole thermal cycle of the 1000°C-oxidation test

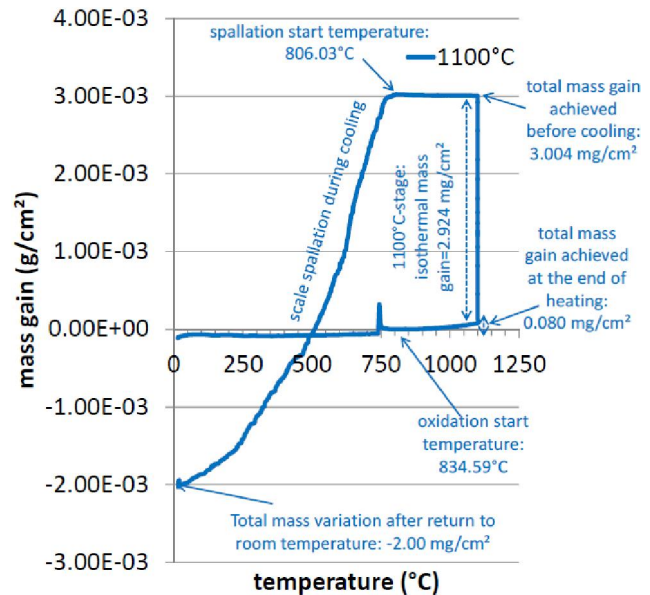


Figure 4 : The {mass gain versus temperature}-plot for the whole thermal cycle of the 1100°C-oxidation test

temperature are presented in Figure 3 for the 1000°C-test, Figure 4 for the 1100°C-test and in Figure 5 for the 1200°C test. In each case arrows show the locations where the values of temperatures or of mass variations were red, as well as the obtained values already presented in the successive tables.

General commentaries

One can now compare the results obtained here with the ones previously obtained for the ternary Co-10Ni-30Cr alloy. Concerning first the temperature of

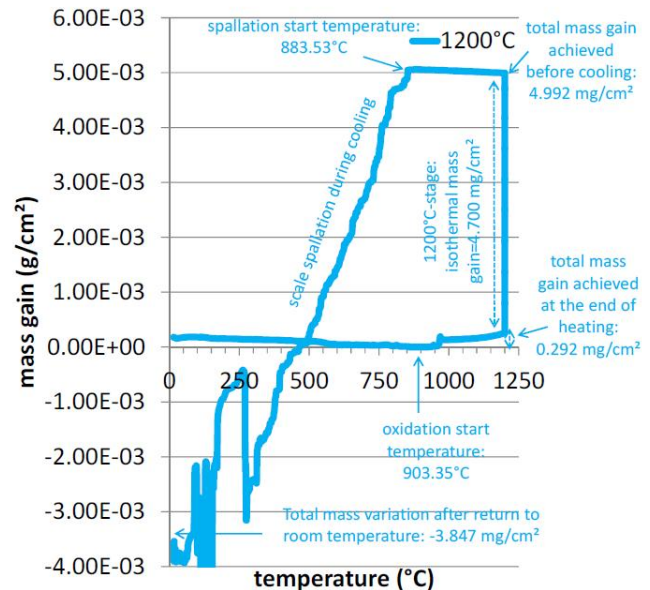


Figure 5 : The {mass gain versus temperature}-plot for the whole thermal cycle of the 1200°C-oxidation test

Full Paper

oxidation start during heating the average values are very close to one another, with here 837.63°C against 839.97°C (in both cases average value calculated from the three heating curves up to 1000, 1100 and 1200°C). One must remind that the 1200°C-heating curve was perturbed, thus it seems preferable to discard the corresponding values. By comparing only the values for the 1000°C-curve and the ones for the 1100°C-curve

it seems that the oxidation of the present alloy started to be detectable at lower temperatures than for the ternary alloy. The presence of the very oxidable element tantalum emerging of surface with the form of carbides has maybe accelerated the oxidation at low temperature. No systematic difference were seen between the two same alloys about the activation energy relative to the linear constant at the beginning of the isothermal stage

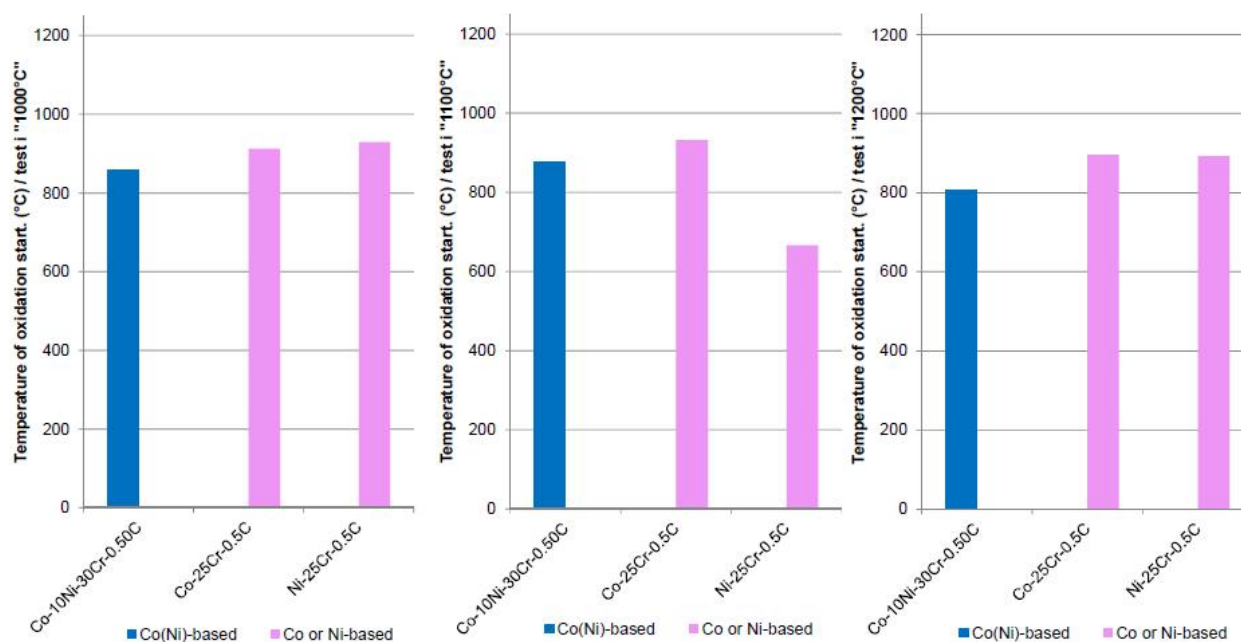


Figure 6: Comparison of the temperatures of oxidation start at heating for the Co-10Ni-30Cr-0.5C alloy (this study), a Co-25Cr-0.5C alloy^[16-18] and a Ni-25Cr-0.5C alloy^[19-21]

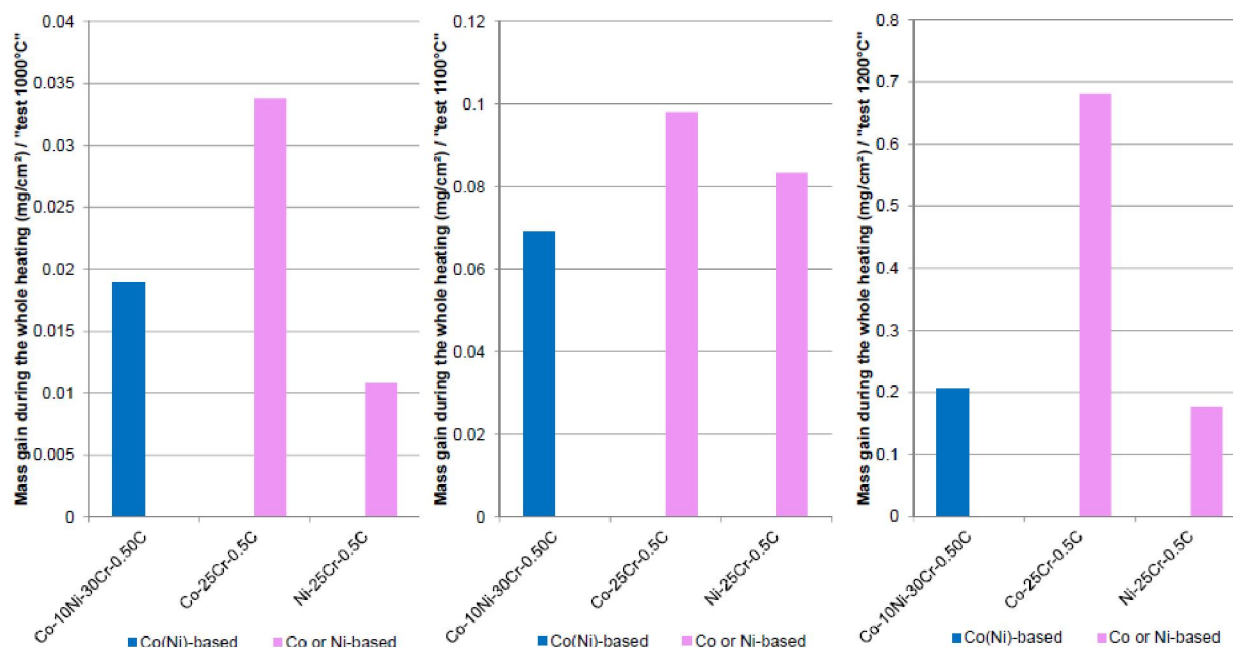


Figure 7: Comparison of the total mass gain achieved during heating for the Co-10Ni-30Cr-0.5C alloy (this study), a Co-25Cr-0.5C alloy^[16-18] and a Ni-25Cr-0.5C alloy^[19-21]

as well as about this linear constant itself. In contrast the total mass gain achieved during heating is higher for the present alloy than for the ternary alloy: +211.1% for heating up to 1000°C, +77.8% for heating up to 1100°C and +93.4% for heating up to 1200°C. The same comments can be done about the isothermal mass gain: +55.6% for the stage at 1000°C, +27.7% for the stage at 1100°C and +6.3% for the stage at 1200°C.

Thus, the relative difference decreases when the stage temperature increases. During the cooling the temperature at which spallation started tended to be lower for the present alloy by comparison to the ternary one. Indeed, if this occurred 53°C higher for the cooling from the 1100°C-stage, spallation took place 30°C lower for cooling from the 1200°C-stage and 107°C lower for the cooling from the 1000°C-stage.

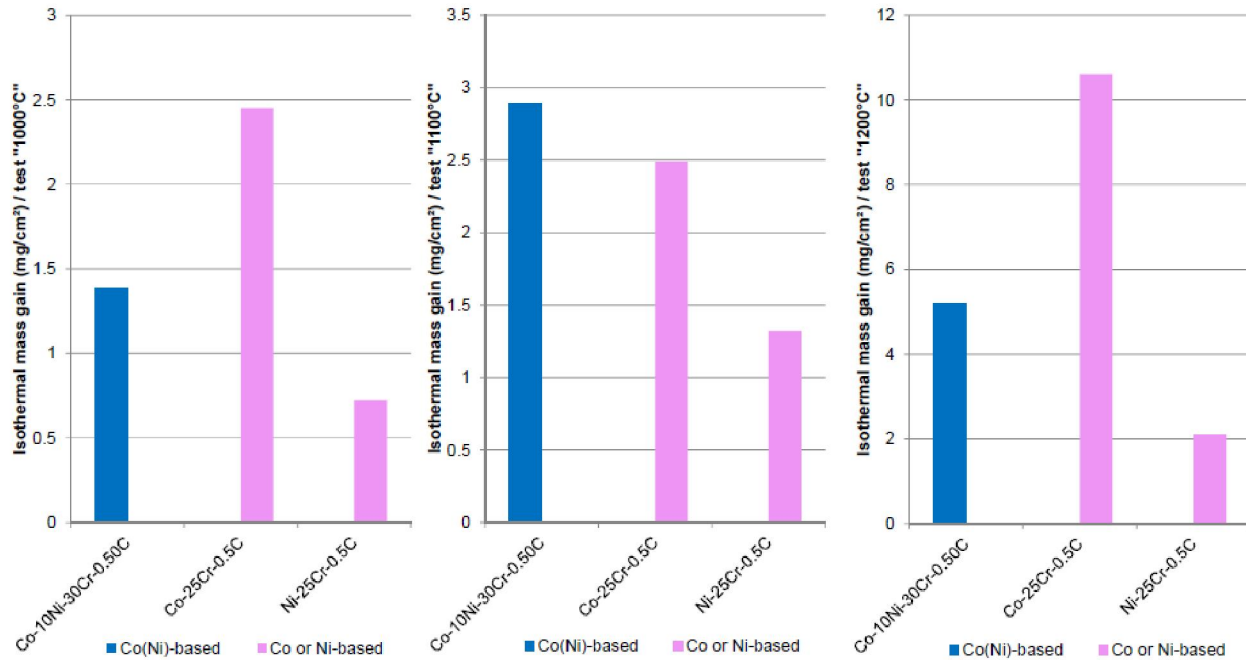


Figure 8 : Comparison of the total mass gain achieved during the isothermal stage for the Co-10Ni-30Cr-0.5C alloy (this study), a Co-25Cr-0.5C alloy^[16-18] and a Ni-25Cr-0.5C alloy^[19-21]

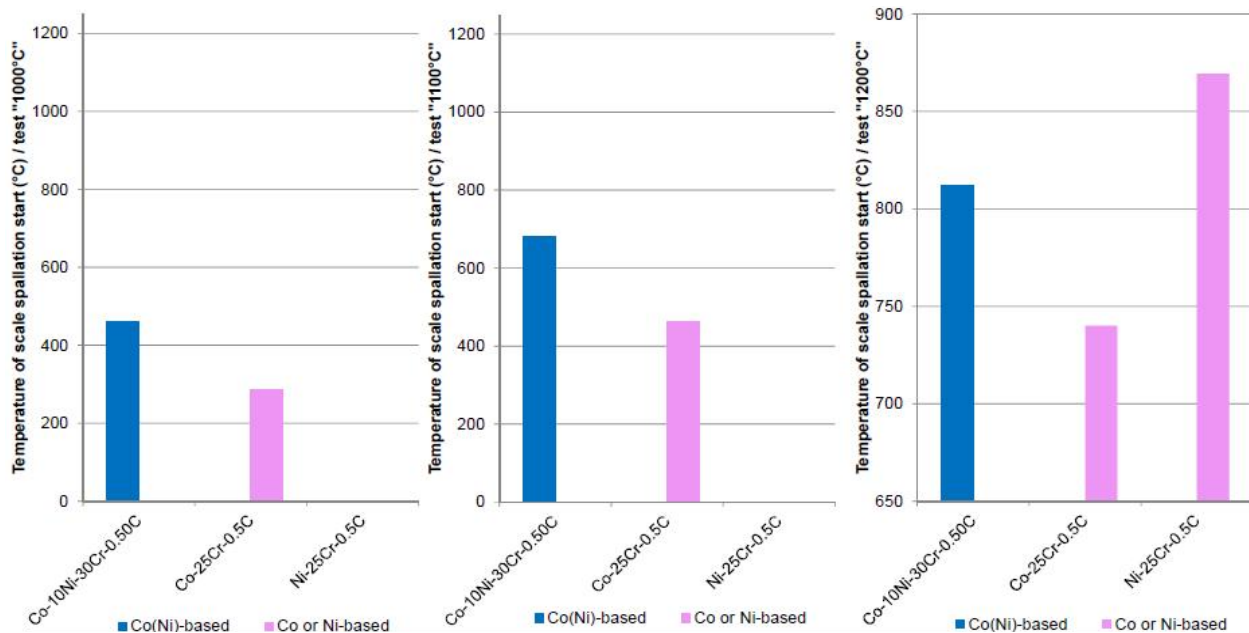


Figure 9 : Comparison of the temperatures of spallation start at cooling for the Co-10Ni-30Cr-0.5C alloy (this study), a Co-25Cr-0.5C alloy^[16-18] and a Ni-25Cr-0.5C alloy^[19-21]

Full Paper

These differences are thus not the same as the ones seen between the {chromium carbides}-containing alloy and same carbide-free ternary one. Indeed, here the presence of carbides more clearly induced sooner start of oxidation during the heating, smaller relative increase in total mass gain during heating and, in contrast, a little higher relative increase in isothermal mass gain. Concerning the cooling, the scale spallation was here too delayed to lower temperatures, but not so later as for the {chromium carbides}-containing alloy. In contrast the total mass variation calculated at room temperature between the initial mass and the final mass of the samples is here significantly lower in absolute value than both the ternary alloy and the {chromium carbides}-containing alloy.

All these parameters characterizing the global oxidation behaviour for the whole thermal cycle does not depend only on the nature of carbides for a given alloy base, but it depends also on the alloy base for a given network of carbides, chromium carbides for example. Thus, to finish, since a Co-10Ni-30Cr-0.5C was studied in this work while other 0.50C-containing alloys rich in chromium (not 30wt.%Cr but 25wt.%Cr) based either on Co or on Ni was subjected to the same oxidation tests and exploitations, it can be interesting to compare them. This was done concerning the oxidation start temperature at heating (Figure 6), the total mass

gain achieved during heating (Figure 7), the isothermal mass gain (Figure 8), the temperature of scale spallation start at cooling (Figure 9) and the final mass variation during the whole thermal stage (Figure 10). In each of these figures the histogram placed on the left corresponds to the tests the stage temperatures of which are 1000°C, the one placed in the middle corresponds to the test at 1100°C and the one placed on the right corresponds to the test at 1200°C.

One can see that these five oxidation characteristics effectively depend on the nature of the matrix. The present Co(Ni)-based alloy (Co-10Ni-30Cr-0.5C) tends starting oxidizing a little sooner than the Co-based one (Co-25Cr-0.5C) and the Ni-based one (Ni-25Cr-0.5C), as visible in Figure 6. One can think that these differences are not really significant. In contrast, concerning the total mass gain achieved during the whole heating, the Co(Ni)-based alloy presents a mass gain which is lower than the Co-based alloy's one and the Ni-based alloy's one.

This is the globally the same order for the isothermal mass gain, except at 1100°C (Figure 8). By considering the temperatures of scale spallation start (Figure 9) it seems that the Co-based alloy spalled off later than the Co(Ni)-based alloy while the Ni-based alloy is the best in this field, except during cooling from 1200°C. In contrast, there is no real link between the temperature

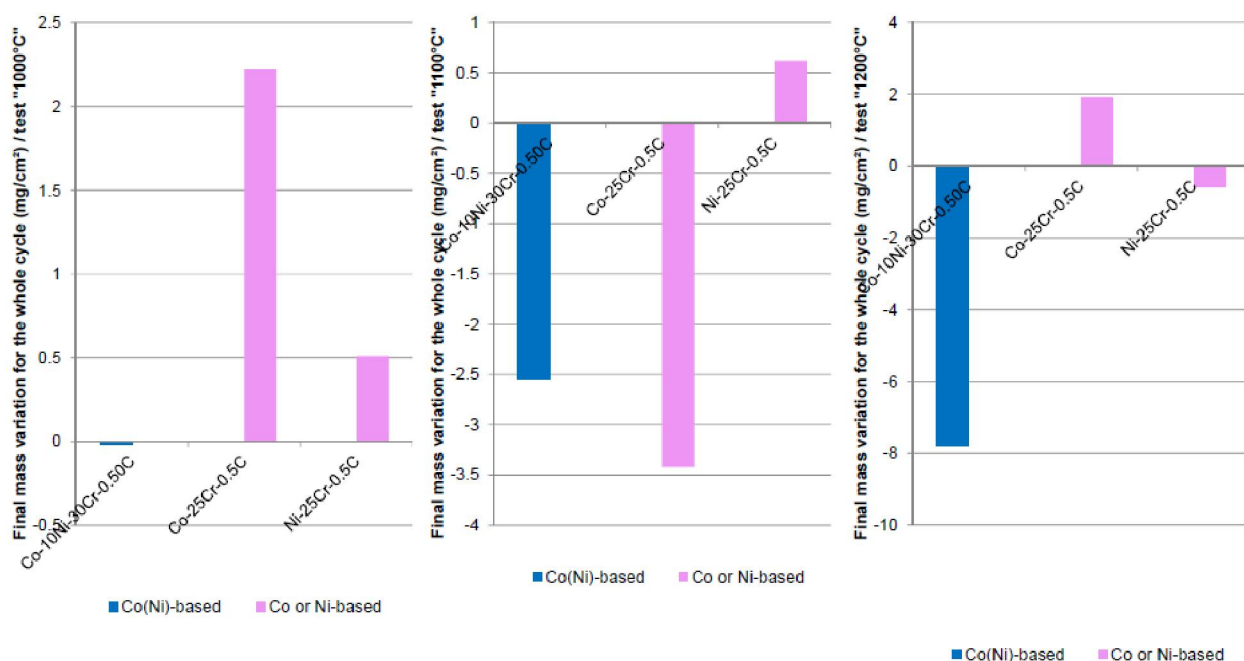


Figure 10 : Comparison of the total mass variation during the whole thermal cycle for the Co-10Ni-30Cr-0.5C alloy (this study), a Co-25Cr-0.5C alloy¹⁶⁻¹⁸ and a Ni-25Cr-0.5C alloy^[19-21]

of spallation start and the final mass loss (Figure 10) since the results are rather scattered.

However it seems that the where cobalt is the most present element in the chemical composition, the corresponding alloys (Co(Ni)-based and Co-based) are able of the best and the worst; this depends on the test temperature. To summarize, there is also a real effect of the base element(s), and on three or four of the precedent criteria the intermediate alloy based on cobalt but containing significant quantity of nickel is situated between the one based on cobalt only and the one based on nickel only.

CONCLUSIONS

In this third and final part of this study the possible influence of the tantalum carbides on the high temperature oxidation behaviour of cobalt-based alloys was evidenced. Their presence exposes tantalum in extreme surface with as consequence a sooner detectable mass gain by oxidation during the heating. This results in a higher mass gain achieved before isothermal oxidation begins. The presence of tantalum carbides also induced an isothermal mass gain rate a little faster. In contrast, during the cooling the TaC, being interdendritic carbides too, tends to improve the resistance of the oxide scale against spallation, but not so efficiently as the chromium carbides in term of spallation start temperature. In contrast the scales were more kept on surface and were more available to protect the alloy for new thermal cycles.

REFERENCES

- [1] C.T.Sims, W.C.Hagel; The superalloys, John Wiley & Sons, New York, (1972).
- [2] A.M.Beltram; Superalloys II-High Temperature Materials for Aerospace Industry Power, John Wiley, New York, 135 (1987).
- [3] E.F.Bradley; Superalloys: A Technical Guide, ASM International, Metals Park, (1988).
- [4] M.J.Donachie, S.J.Donachie; Superalloys: A Technical Guide, (2nd Edition), ASM International, Materials Park, (2002).
- [5] P.Berthod, S.Michon, L.Aranda, S.Mathieu, J.C.Gachon; Calphad, **27**, 353 (2003).
- [6] P.Berthod, S.Raude, A.Chiaravalle; Annales de Chimie – Science des Matériaux, **31(2)**, 237 (2006).
- [7] P.Berthod, Y.Hamini, L.Aranda, L.Héricher; Calphad, **31**, 351 (2007).
- [8] P.Berthod, Y.Hamini, L.Héricher, L.Aranda; Calphad, **31**, 361 (2007).
- [9] P.Berthod, L.Aranda, C.Vébert, S.Michon; **28**, 159 (2004).
- [10] S.Michon, L.Aranda, P.Berthod, P.Steinmetz; La Revue de Métallurgie – C.I.T. Science et Génie des Matériaux, **12**, 1031 (2004).
- [11] P.Berthod, C.Heil, L.Aranda; Journal of Alloys and Compounds, **504**, 243 (2010).
- [12] P.Berthod, L.Aranda, C.Heil; The Open Corrosion Journal, **2**, 150 (2009).
- [13] A.Navet, A.Leroy, T.Schweitzer, L.Aranda, P.Berthod; Materials Science: An Indian Journal, submitted.
- [14] P.Berthod, L.Aranda, T.Schweitzer, A.Leroy, A.Navet; Materials Science: An Indian Journal, submitted.
- [15] P.Berthod, L.Aranda, T.Schweitzer, A.Navet, A.Leroy; Materials Science: An Indian Journal, submitted.
- [16] P.Berthod, E.Conrath; Materials Science: An Indian Journal, **10(1)**, 38 (2013).
- [17] E.Conrath, P.Berthod; Materials Science: An Indian Journal, in press.
- [18] P.Berthod, E.Conrath; Materials Science: An Indian Journal, in press.
- [19] E.Conrath, P.Berthod; Materials Science: An Indian Journal, **10(1)**, 30 (2013).
- [20] P.Berthod, E.Conrath; Materials Science: An Indian Journal, in press.
- [21] E.Conrath, P.Berthod; Materials Science: An Indian Journal, in press.